

Research Article

Fabrication of Si/SiO₂ Superlattice Microwire Array Solar Cells Using Microsphere Lithography

Shigeru Yamada,¹ Shinsuke Miyajima,² and Makoto Konagai^{1,3}

¹Japan Science and Technology Agency (JST), Fukushima Renewable Energy Institute (FREA), Koriyama, Fukushima 963-0215, Japan

²Department of Physical Electronics, Tokyo Institute of Technology, Meguro, Tokyo 152-8552, Japan

³Advanced Research Laboratories, Tokyo City University, Setagaya, Tokyo 158-0082, Japan

Correspondence should be addressed to Shigeru Yamada; sigeru.yamada@pb.jst.jp

Received 21 July 2016; Accepted 27 September 2016

Academic Editor: Xiaopeng Li

Copyright © 2016 Shigeru Yamada et al. This is an open access article distributed under the Creative Commons Attribution License, which permits unrestricted use, distribution, and reproduction in any medium, provided the original work is properly cited.

A fabrication process for silicon/silicon dioxide (Si/SiO₂) superlattice microwire array solar cells was developed. The Si/SiO₂ superlattice microwire array was fabricated using a microsphere lithography process with polystyrene particles. The solar cell shows a photovoltaic effect and an open-circuit voltage of 128 mV was obtained. The limiting factors of the solar cell performance were investigated from the careful observations of the solar cell structures. We also investigated the influence of the microwire array structure on light trapping in the solar cells.

1. Introduction

The development of crystalline silicon (c-Si) solar cells has a long history and a conversion efficiency of 25.6% has recently been achieved by back-contact silicon heterojunction cells [1]. However, the theoretical conversion efficiency limit of a c-Si single-junction solar cell under 1 sun irradiation is lower than 30% according to the Shockley-Queisser limit [2, 3]. Some novel techniques have been proposed to realize solar cells with higher conversion efficiency than the theoretical limit [4–6]. Examples of solar cells fabricated using the proposed techniques are multiple exciton generation effect solar cells, intermediate-band solar cells, and hot-carrier solar cells. In addition, tandem solar cells or multijunction solar cells are also promising for exceeding the theoretical conversion efficiency limit of single-junction solar cells [7]. Multijunction solar cells can reduce transmission losses and thermal relaxation losses by using two or more absorber materials. In the case of a double-junction solar cell with a c-Si bottom cell, the optimum bandgap for the absorber material in the top cell is approximately 1.7 eV. Si nanomaterials, such as silicon quantum wells, silicon quantum wires, and silicon quantum dots, are attractive materials for realizing wide-bandgap Si-related materials based on the quantum size effect

[8–11]. A silicon/silicon dioxide superlattice (Si/SiO₂ SL), which is one of the Si nanomaterials, has been investigated for applications to wide-bandgap materials by many researchers for many years. In particular, the bandgap shift in Si/SiO₂ SLs has been confirmed by optical measurements, such as photoluminescence spectrum and absorption spectrum measurements [12–15]. However, the research on the electrical properties of Si/SiO₂ solar cells is at an early stage, and the confirmation of a bandgap shift from electrical measurements has hardly been reported. On the other hand, theoretical calculations of the electrical properties have been carried out using several methods, such as by combining first-principle calculations and a drift-diffusion transport model and by the nonequilibrium Green's function method [16–18]. The solar cell performance is quite sensitive to the thickness of the SiO₂ layers in a Si/SiO₂ SL. The carrier localization in the SL, where an electrical field is applied, due to the Wannier-Stark effect can be a problem [19, 20]. Nevertheless, high-efficiency c-Si solar cells with a tunnel oxide passivated contact have been reported recently [21, 22], suggesting that the quantum effect can be applied to solar cells. Solar cells utilizing the quantum tunneling effect through high barrier layers, similarly to those using the quantum size effect, are promising and should be actively investigated.

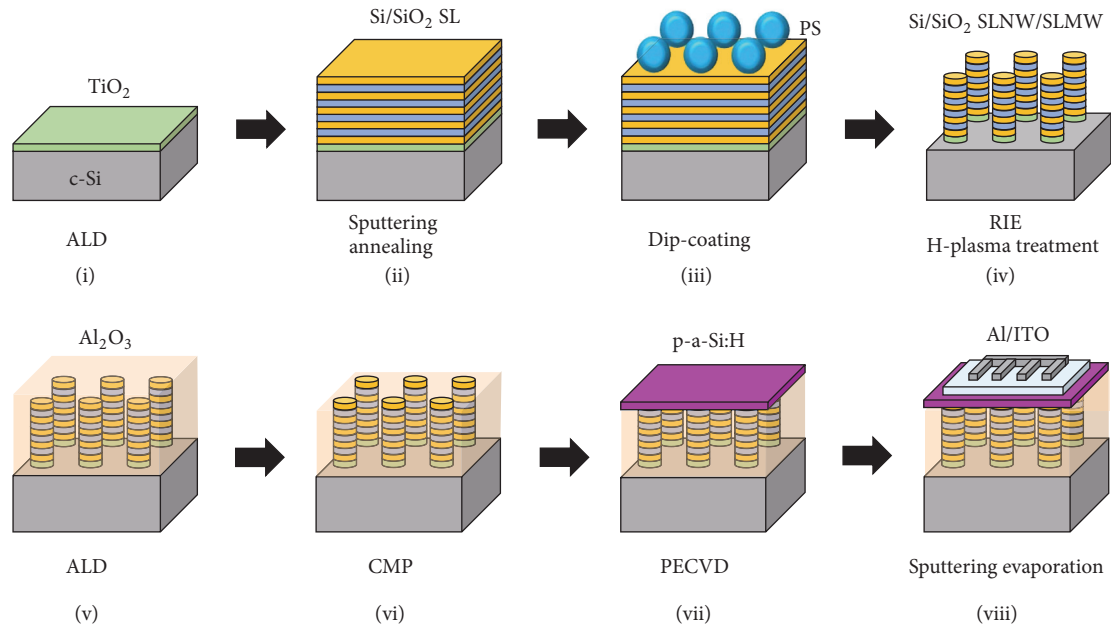


FIGURE 1: Schematic diagram of fabrication procedure of Si/SiO₂ SLNW or SLMW solar cells.

We have proposed silicon superlattice microwire (SLMW) structures. In this structure, the SL introduces the quantum confinement effect into solar cells. A MW array realizes light trapping in solar cells. An advantage of the wire structures is that the thickness of a Si/SiO₂ SL absorber layer can be reduced due to the optical confinement effect. The reduction of the SL thickness will contribute to the reduction of series resistance of the SL absorber layer. The optimum length and diameter for a Si/SiO₂ wire should be 1 μm to 2 μm and 500 nm to 2 μm, respectively, as previously reported [23]. From the viewpoint of quantum confinement, silicon superlattice nanowire (SLNW) is also a promising structure. However, the optical confinement effect of SLMW is expected to be superior to that of SLNW. In this article, the fabrication of Si/SiO₂ SLMW array solar cells using microsphere lithography techniques is reported. Furthermore, the problems of the solar cells were analyzed in detail.

2. Materials and Methods

The step-by-step fabrication process of Si/SiO₂ SLMW array solar cells is shown in Figure 1. Titanium dioxide (TiO₂) films were deposited on heavily phosphorus-doped Si substrates ($\rho = 0.0007\text{--}0.0015\ \Omega\cdot\text{cm}$) by atomic layer deposition (ALD). Si/SiO₂ SLs were prepared on the TiO₂-coated Si substrates by magnetron sputtering and subsequent annealing. A Si target (99.999%) was used for the sputtering. Argon (Ar) gas was used for the Si layer deposition and a mixture of Ar and oxygen (O₂) was used for the deposition of the SiO₂ layer. The deposited Si layer was amorphous silicon (a-Si). The periodic structure of the a-Si and SiO₂ layers was prepared by flowing Ar and a mixture of Ar and O₂ periodically. The thickness of each layer can be tuned by controlling the flowing time of each gas. In this study, SL films with 7.9 nm thick Si layers

and 2.2 nm thick SiO₂ layers were prepared. The number of periods of the SL was 108 so that the total SL thickness was approximately 1 μm. The deposition pressure, deposition temperature, and plasma power density were 1.0 Pa, 25°C, and 2.36 W/cm², respectively. The films were annealed at 1000°C for 2 h under a forming gas (N₂ : H₂ = 97% : 3%) atmosphere to crystallize the a-Si layers in the SLs. The SL after the thermal annealing can be more structurally and thermally stable. The SL film was exposed to ozone in a UV-ozone cleaner to increase the wettability on the surface. Then, the SL film was dipped into 2 μm diameter polystyrene- (PS-) particle-dispersed water, and the SL film was vertically lifted up under dry air. This process resulted in periodically aligned PS particles on the SL film. The SL films on which PS particles were periodically aligned were etched by reactive ion etching (RIE) using tetrafluoromethane (CF₄) gas, resulting in the SLMW structure. Here, half of the film was covered with a mask to prepare flat-type SL solar cells as reference cells on the same substrate. Then, the SLMW film was exposed to hydrogen plasma at 500°C to reduce the defect density in the SL layer. Subsequently, the films were covered with Al₂O₃ by ALD to prevent leakage through the front electrodes to the c-Si substrate. To make a contact at the front side, Al₂O₃ deposited on the top of the SLMW was selectively removed by chemical mechanical polishing (CMP). After cleaning by hot acetone and a mixture of sulfuric acid and hydrogen peroxide (H₂SO₄ : H₂O₂ = 1 : 3), p-type boron-doped hydrogenated amorphous silicon (p-a-Si:H) films were deposited by plasma-enhanced chemical vapor deposition (PECVD), indium tin oxide (ITO) films were deposited by magnetron sputtering, and aluminum electrodes were deposited using an evaporator. The solar cells were characterized by dark-IV and photo-IV measurements under 1 sun irradiation at 25°C with a King Design KD-SACL-K solar simulator

and an Agilent B1500A semiconductor device analyzer. The wire-array structures and solar cell structures were observed by field-emission scanning electron microscopy (FE-SEM) with a Hitachi SU8230 microscope, transmission electron microscopy (TEM) with a JEOL JEM-ARM200F microscope, and scanning transmission electron microscopy (STEM) with a Hitachi HD-2700 microscope. SL films and SLMW array films were also prepared on quartz substrates to measure the transmittance and reflectance, which were measured by ultraviolet-visible (UV-VIS) spectroscopy with a Shimadzu SolidSpec-3700 spectrometer using an integrating sphere. The dopant diffusion barrier effect of a TiO_2 layer between the c-Si substrate and the SL layer was investigated by secondary ion mass spectroscopy (SIMS) with a CAMECA IMS-7f spectrometer.

3. Results and Discussion

3.1. Dopant Diffusion Barrier Layer. We selected heavily phosphorus-doped c-Si as the substrate in the solar cell structure since it is thermally stable and conductive and has a short minority-carrier lifetime. The short minority-carrier lifetime prohibits the contribution of photogenerated carriers in the c-Si substrate to the photocurrent of the solar cell. However, the phosphorus diffusion from the c-Si substrate into the SL layer during the annealing is a problem. Some approaches, such as the detachment of a film from the substrate and the etching of the substrate, can be effective for avoiding the problem of impurity diffusion [24, 25]. Another approach is the insertion of a thin TiO_2 layer as a barrier layers preventing phosphorus dopant impurity diffusion between the substrate and the SL layer as reported in [26]. Therefore, an ultrathin TiO_2 layer was prepared on a c-Si substrate by ALD and its diffusion barrier effect was investigated. Figure 2 shows depth profiles of the phosphorus concentrations in the Si/SiO₂ SL/c-Si and Si/SiO₂ SL/TiO₂/c-Si structures measured by SIMS, where the thickness of the TiO_2 layer was approximately 4 nm. For both profiles, the peak appearing at the interface between the Si/SiO₂ SL layer and the c-Si substrate originates from the matrix effect. The detection limit of phosphorus in this measurement system is $1 \times 10^{15} \text{ cm}^{-3}$. The penetration lengths of phosphorus into the SL layer are different for both profiles. For the profile without a TiO_2 layer, the phosphorus concentration gradually decays and approaches the detection limit at the depth of approximately 400 nm. On the other hand, for the profile with a 4 nm thick TiO_2 layer, the phosphorus concentration drastically decays and the diffusion length is 70 to 80 nm. From these results, TiO_2 prepared by ALD can be used as a blocking layer against phosphorus diffusion during the 1000°C-annealing process.

3.2. Fabrication of SLMW Array. A surface SEM image of a PS-coated SL before RIE is shown in Figure 3(a). Uniform single-layer PS-particle arrays were successfully prepared on the SL films in an area as wide as 1 cm^2 . Close packing alignments, point defects with vacancies or impurities, and line defects can be seen, similar to the case of a polycrystalline structure. The influence of these defects on the electrical

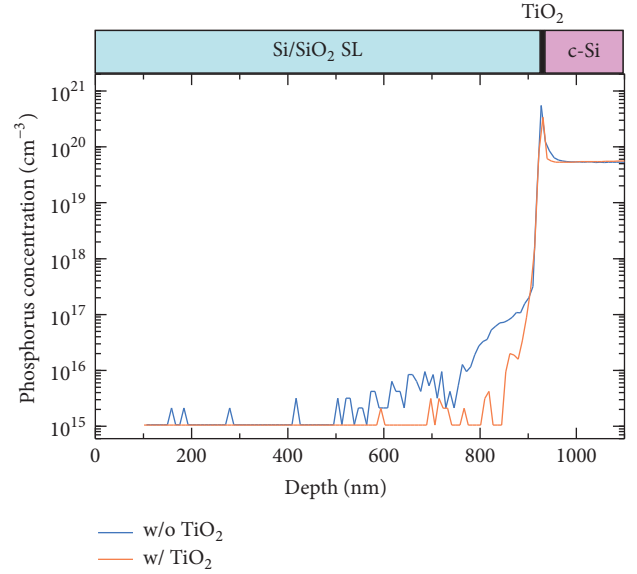


FIGURE 2: Depth profiles of phosphorus concentrations in the structures with and without a TiO_2 layer evaluated by SIMS measurements.

properties and optical properties is considered to be negligible. A surface SEM image of a SLMW array is shown in Figure 3(b). The circles correspond to the top surfaces of SLMWs. The alignment and the diameters of the SLMWs are reflected by those of the PS particles. A cross-sectional SEM image of a SLMW is shown in Figure 3(c). The SLMW has a tapered shape, whose top diameter and bottom diameter can be estimated to be approximately $1.2 \mu\text{m}$ and $1.8 \mu\text{m}$, respectively. The difference between the diameters of the top area and bottom area is due to the reduction of the diameter of the PS particles during the RIE process. On the assumption that PS particles are etched from only the top surface, the shape function of a SLMW can be represented as

$$T(r; t) = \begin{cases} R_f \left(t - \frac{1}{R_s} \sqrt{D^2 - 4r^2} \right), & t > \frac{1}{R_s} \sqrt{D^2 - 4r^2} \\ 0, & t \leq \frac{1}{R_s} \sqrt{D^2 - 4r^2}, \end{cases} \quad (1)$$

where D , R_s , and R_f denote the diameter of a PS particle, the etching rate of a PS particle, and the etching rate of a Si/SiO₂ SL, respectively. Also, r and t mean the distance from the center of a SLMW and the etching time, respectively. The dashed line depicted in Figure 3(c) represents the fitting curve of a SLMW shape based on (1). The etching selectivity, namely, R_f/R_s , estimated from the curve is 0.59. This means that if the thickness of a Si/SiO₂ SL is more than 0.59 times as large as the diameter of a PS particle, the PS particle disappears before the SL film is completely etched. The $2 \mu\text{m}$ diameter PS particles are sufficiently large to obtain a SLMW array with a depth and diameter of approximately $1 \mu\text{m}$.

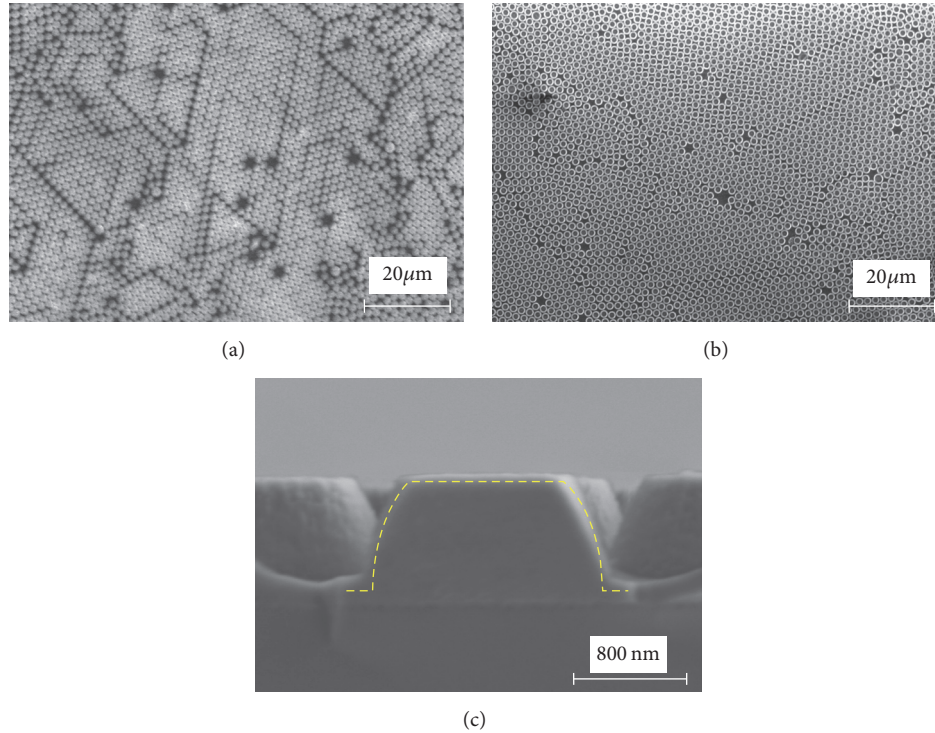


FIGURE 3: (a) Surface SEM image of a PS-particle-array-coated Si/SiO₂ SL. (b) Surface SEM image of a Si/SiO₂ SLMW array after RIE. (c) Cross-sectional SEM image of a Si/SiO₂ SLMW. The yellow dashed line represents the fitting line based on the wire shape function given by (1).

The transmittance (T), reflectance (R), and absorbance (A) spectra of a flat SL and a SLMW array are shown in Figure 4. Here, the absorbance is calculated by

$$A = 100 - R - T. \quad (2)$$

The transmittance spectrum for a SLMW is lower than that for the flat SL in the wavelength region longer than 550 nm. The fluctuation of the spectrum due to optical interference also decreases. This is probably due to the optical confinement in the MW structure. On the other hand, the reflectance spectrum for the SLMW in the wavelength region between 400 nm and 700 nm is lower than that for the flat SL. This is due to the antireflection effect of the MW structure. As a result, the absorption spectrum for the SLMW array is higher than that for the flat SL in a wide wavelength region. The enhancement of the absorption spectrum can contribute to increasing the effective optical length. Here, it should be noted that the absorption for both cases in the long wavelength region larger than the bandgap energy of a SL should be zero. The fluctuations in the spectra are artificially produced peaks due to fluctuations of the angle and/or the gap distance between the sample and the integrating sphere, which is especially sensitive for textured samples.

3.3. SLMW Array Solar Cells. Figure 5(a) shows the dark-IV and photo-IV characteristics for a flat SL solar cell and Figure 5(b) shows the dark-IV and photo-IV characteristics for a SLMW array solar cell fabricated using the fabrication process shown in Figure 1. The open-circuit voltage (V_{oc})

and short-circuit current density (J_{sc}) for the flat SL solar cell were 107 mV and 7.1×10^{-5} mA/cm², respectively. On the other hand, V_{oc} and J_{sc} for the SLMW solar cell were 128 mV and 1.4×10^{-4} mA/cm², respectively. The photovoltaic effect was obtained for both the flat SL and the SLMW. The difference between the leakage currents of the solar cells is not so large, which means that the spaces between the SLMWs were insulated with Al₂O₃ prepared by ALD and the leakage paths were not formed. These results indicate that our fabrication process is basically applicable to solar cell fabrication. However, the solar cell performance is still low. The diode parameters, the series resistance (R_s), the shunt resistance (R_{sh}), the reverse saturation current density (J_0), and the ideal diode factor (n) for a flat SL cell and a SLMW cell were estimated by fitting the dark-IV curves with ideal one diode model. J_0 , R_s , R_{sh} , and n were 8.9×10^{-7} mA/cm², 1.3×10^4 Ωcm², 4.0×10^6 Ωcm², and 2.7 for the SLNW cell and 2.5×10^{-7} mA/cm², 4.0×10^4 Ωcm², 3.2×10^6 Ωcm², and 2.8 for the SL cell, respectively. Here, R_s and n should be noted. The diode factor n is greater than 2.0, which suggests that high barriers against carriers are existing in the solar cell and the barriers lead to small V_{oc} [27, 28]. Besides, such high series resistances significantly affect J_{sc} . The poor J_{sc} is probably due to the very high series resistance, and the poor V_{oc} is associated with the poor ohmic contact at the p-layer/SL layer.

To examine the solar cells in more detail, the cross-sectional structure of the solar cells was investigated. Figure 6 shows cross-sectional TEM images of an SLMW array solar cell. Figure 6(a) shows the whole region of the SLMW

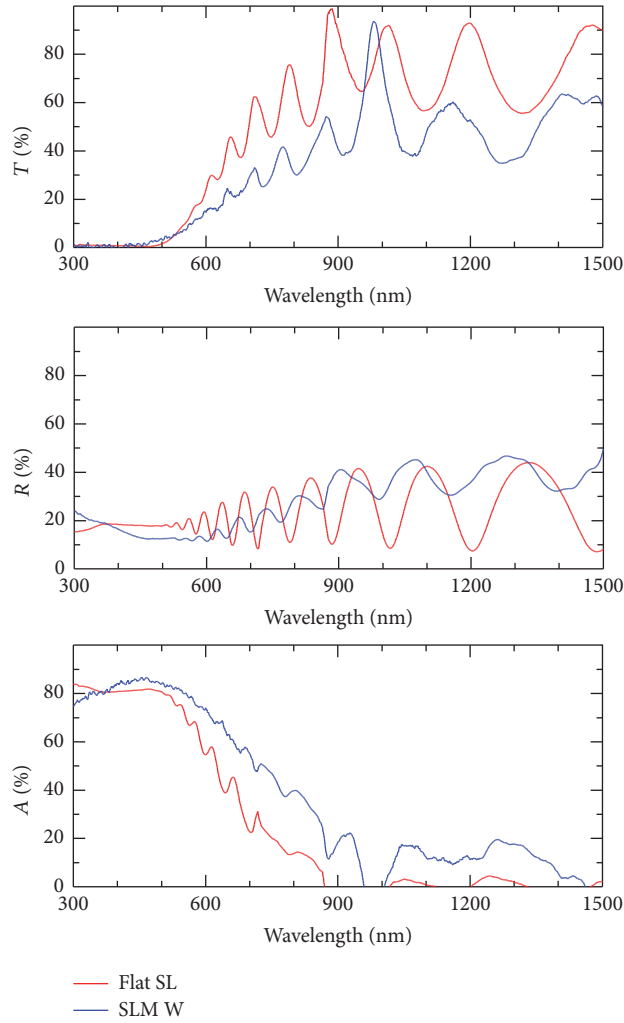


FIGURE 4: Transmittance, reflectance, and absorbance of a flat SL film and a SLMW array film deposited on quartz substrates. The red and blue lines correspond to the flat SL and the SLMW array, respectively.

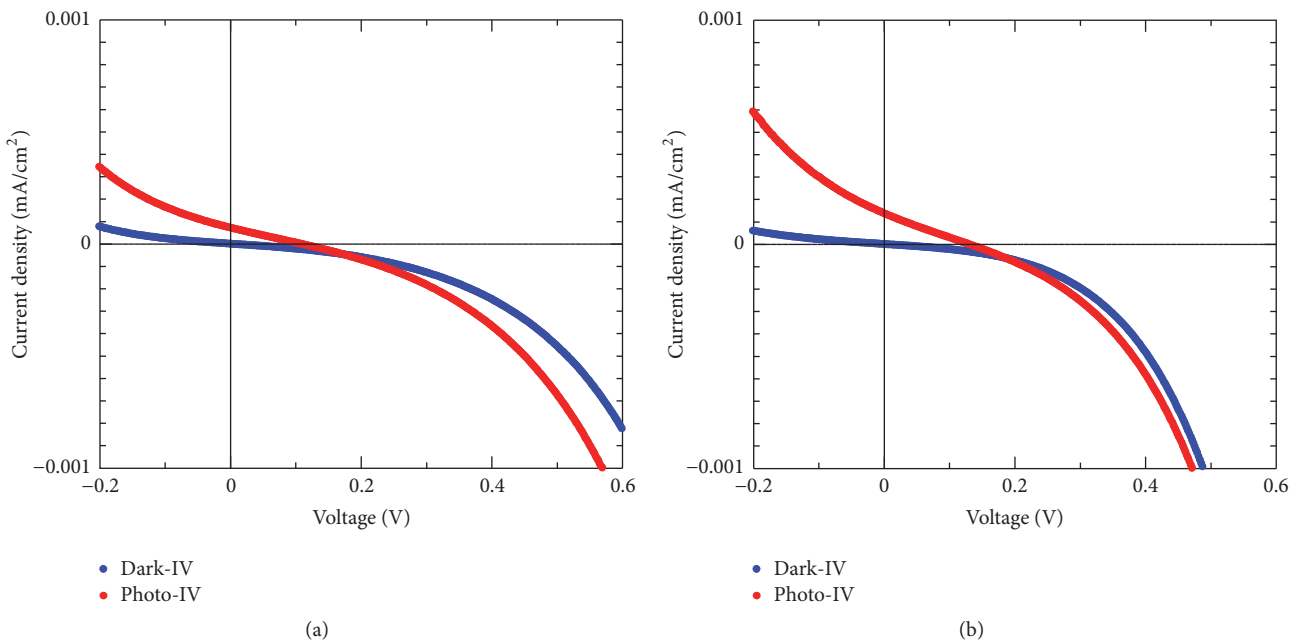


FIGURE 5: Dark-IV and photo-IV characteristics for (a) flat SL solar cell and (b) SLMW array solar cell.

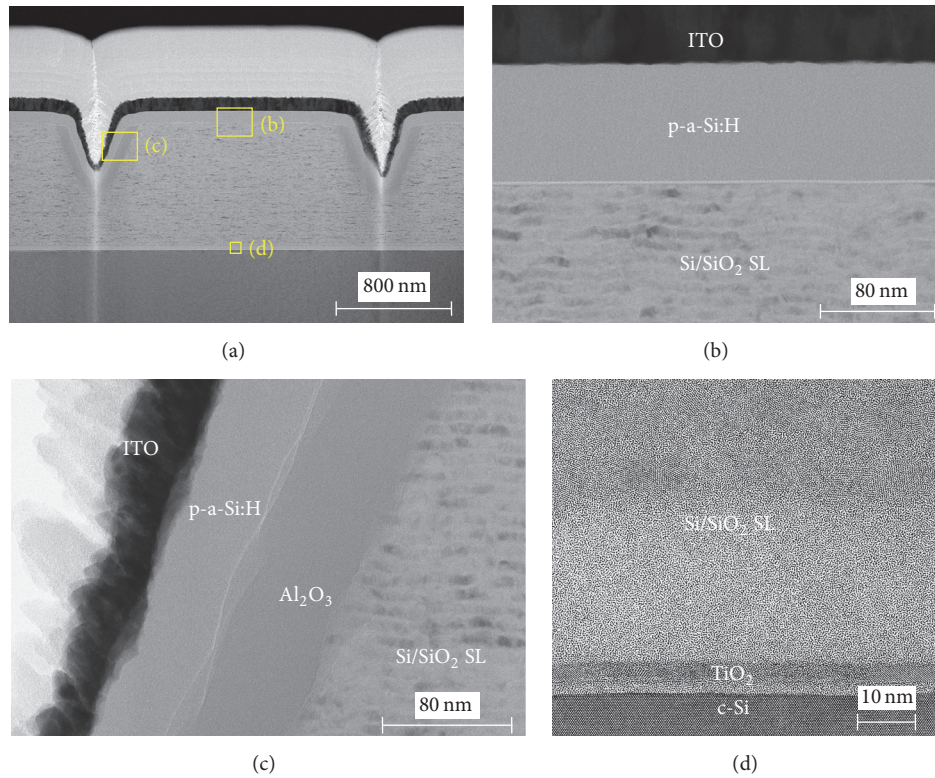


FIGURE 6: Cross-sectional STEM images of (a) whole area of a SLMW, (b) magnified image of top region of the SLMW, and (c) magnified image of side region of the SLMW. (d) Cross-sectional magnified TEM image of bottom region of the SLMW.

structure observed by STEM. The thick white layer deposited on the top of the solar cell structure is the supporting layer used for the preparation of a TEM sample. The dark layer is the ITO layer. A layered structure can be seen in the SL layer. Figures 6(b), 6(c), and 6(d) show magnified images of the top area of the SLMW, the side area of the SLMW, and the bottom area of the SLMW, respectively. As shown in Figure 6(c), an Al_2O_3 layer covers the side of the SLMW, and the SLMW is isolated from the p-type a-Si:H layer and ITO layer. On the other hand, in the top area of the SLMW, the Al_2O_3 layer has been removed and a p-type a-Si:H layer has been deposited on the SLMW as shown in Figure 6(b). Furthermore, the surface is quite flat after the CMP process. Therefore, the contact with the p-layer is considered to have only formed on the top area of the SLMW array. However, an ultrathin white layer can be seen between the p-type layer and the SL layer, implying that a thin oxide layer still remains. The samples were cleaned by a mixture of sulfuric acid and hydrogen peroxide, resulting in the formation of the thin oxide layer. In the bottom area of the SLMW, a TiO_2 layer can be seen on the c-Si substrate as shown in Figure 6(d). An oxide layer also exists between the TiO_2 layer and the c-Si substrate, which is due to the surface oxidation in the early phase of the ALD deposition process. Also, a thick oxide layer, whose thickness is around 25 nm to 30 nm, exists on the TiO_2 layer, and several nc-Si layers in the SL are broken. This is attributed to the instability of the oxygen

partial pressure in the atmosphere in the early phase of SL deposition. Such oxidized layers can contribute to the high series resistance. Other possible reasons for the high series resistance are the resistance in the ITO layer deposited on the wire structure. The ITO is thinner on the side of the SLMWs if the trenches of the SLMWs are not completely embedded. Since the resistances for poly-Si solar cells prepared with a poly-Si layer in place of a SL were as high as those for SL solar cells, one can conclude that such high resistances mainly originate from the unintentional formation of the oxidized layer during the fabrication process. These problems can be resolved by careful cleaning and improving the settings of each layer deposition process.

The reflectance of the SLMW solar cell structure was also investigated to clarify the advantage of a wire structure. Figure 7 shows the reflectance spectra of a flat SL solar cell and a SLMW cell structure with and without an ITO layer. For the flat SL solar cell, the reflectance with ITO is lower than that without ITO since the ITO layer acts as an antireflection layer. Similarly, for the SLMW solar cell, the reflectance with ITO is lower than that without ITO. The reflectance for the SLMW solar cell is lower than that of the flat SL solar cell. In addition, optical interference is suppressed for the SLMW solar cell, implying that light trapping occurred in the SLMW solar cell. While the ITO layer has an antireflection effect, it is enhanced by the wire structures, and the enhancement of the photocurrent can be expected.

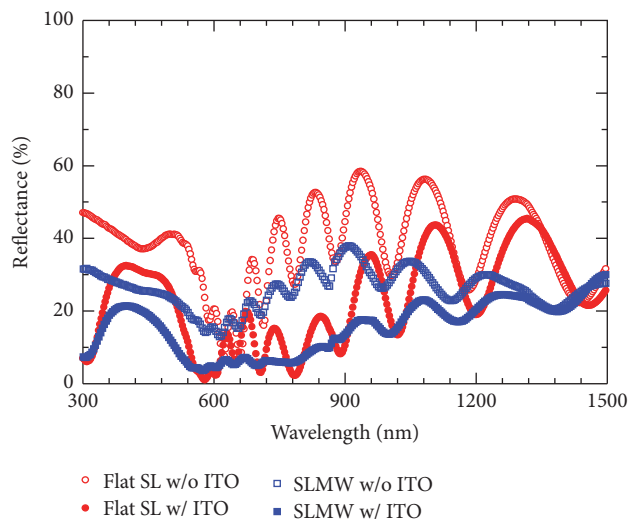


FIGURE 7: Reflectance spectra of a flat SL solar cell and a SLMW solar cell structure with and without an ITO layer.

4. Conclusions

We prepared Si/SiO₂ SLMW array films and solar cells. The photovoltaic effect was confirmed from the SLMW solar cell as well as from the flat SL solar cell. Careful observations of the solar cell structure revealed that unintentional oxidized layers at the front and rear interface of the SL layer lead to the very high series resistance of our devices. If the high series resistance resulting from the oxidized layers is removed, the enhancement of J_{sc} by the optical confinement effect can be expected.

Competing Interests

The authors declare that there is no conflict of interests regarding the publication of this paper.

Acknowledgments

The authors would like to express sincere thanks to the Ministry of Education, Culture, Sports, Science and Technology (MEXT), Japan, FUTURE-PV Innovation for their support. Also, the authors would like to thank Shintaro Kubo for the preparation of samples.

References

- [1] K. Masuko, M. Shigematsu, T. Hashiguchi et al., "Achievement of more than 25% conversion efficiency with crystalline silicon heterojunction solar cell," *IEEE Journal of Photovoltaics*, vol. 4, no. 6, pp. 1433–1435, 2014.
- [2] W. Shockley and H. J. Queisser, "Detailed balance limit of efficiency of p - n junction solar cells," *Journal of Applied Physics*, vol. 32, no. 3, pp. 510–519, 1961.
- [3] T. Tiedje, E. Yablonovitch, G. D. Cody, and B. G. Brooks, "Limiting efficiency of silicon solar cells," *IEEE Transactions on Electron Devices*, vol. ED-31, no. 5, pp. 711–716, 1984.
- [4] A. J. Nozik, M. C. Beard, J. M. Luther, M. Law, R. J. Ellingson, and J. C. Johnson, "Semiconductor quantum dots and quantum dot arrays and applications of multiple exciton generation to third-generation photovoltaic solar cells," *Chemical Reviews*, vol. 110, no. 11, pp. 6873–6890, 2010.
- [5] Y. Okada, N. J. Ekins-Daukes, T. Kita et al., "Intermediate band solar cells: recent progress and future directions," *Applied Physics Reviews*, vol. 2, no. 2, Article ID 021302, 2015.
- [6] D. Knig, K. Casalenuovo, Y. Takeda et al., "Hot carrier solar cells: principles, materials and design," *Physica E*, vol. 42, no. 10, pp. 2862–2866, 2010.
- [7] A. D. Vos, "Detailed balance limit of the efficiency of tandem solar cells," *Journal of Physics D: Applied Physics*, vol. 13, no. 5, pp. 839–846, 1980.
- [8] Y. Takahashi, T. Furuta, Y. Ono, T. Ishiyama, and M. Tabe, "Photoluminescence from a silicon quantum well formed on separation by implanted oxygen substrate," *Japanese Journal of Applied Physics*, vol. 34, no. 2, pp. 950–954, 1995.
- [9] X. Zhao, C. M. Wei, L. Yang, and M. Y. Chou, "Quantum confinement and electronic properties of silicon nanowires," *Physical Review Letters*, vol. 92, no. 23, pp. 236805–1, 2004.
- [10] Y. Kurokawa, S. Tomita, S. Miyajima, A. Yamada, and M. Konagai, "Photoluminescence from silicon quantum dots in Si quantum dots/amorphous SiC superlattice," *Japanese Journal of Applied Physics*, vol. 46, no. 33–35, pp. L833–L835, 2007.
- [11] G. Conibeer, M. Green, E.-C. Cho et al., "Silicon quantum dot nanostructures for tandem photovoltaic cells," *Thin Solid Films*, vol. 516, no. 20, pp. 6748–6756, 2008.
- [12] D. J. Lockwood, Z. H. Lu, and J. Baribeau, "Quantum Confined luminescence in Si/SiO₂ superlattices," *Physical Review Letters*, vol. 76, no. 3, pp. 539–541, 1996.
- [13] M. Zacharias, J. Heitmann, R. Scholz, U. Kahler, M. Schmidt, and J. Bläsing, "Size-controlled highly luminescent silicon nanocrystals: a SiO/SiO₂ superlattice approach," *Applied Physics Letters*, vol. 80, no. 4, pp. 661–663, 2002.
- [14] J. Lopez-Vidrier, S. Hernandez, A. M. Hartel et al., "Structural and optical characterization of size controlled silicon nanocrystals in SiO₂/SiO_xN_y multilayers," *Energy Procedia*, vol. 10, pp. 43–48, 2011.
- [15] S. Yamada, M. Konagai, and S. Miyajima, "Investigation of the optical absorption in Si/SiO₂ superlattice for the application to solar cells," *Japanese Journal of Applied Physics*, vol. 55, Article ID 04ES06, 2016.
- [16] T. Kirchartz, K. Seino, J.-M. Wagner, U. Rau, and F. Bechstedt, "Efficiency limits of Si/SiO₂ quantum well solar cells from first-principles calculations," *Journal of Applied Physics*, vol. 105, no. 10, Article ID 104511, 2009.
- [17] U. Aeberhard, "Theory and simulation of photogeneration and transport in Si-SiO_x superlattice absorbers," *Nanoscale Research Letters*, vol. 6, article 242, 2011.
- [18] U. Aeberhard, "Effective microscopic theory of quantum dot superlattice solar cells," *Optical and Quantum Electronics*, vol. 44, no. 3–5, pp. 133–140, 2012.
- [19] R. Tsu and G. Döhler, "Hopping conduction in a 'superlattice,'" *Physical Review B*, vol. 12, no. 2, pp. 680–686, 1975.
- [20] A. Wacker, "Semiconductor superlattices: a model system for nonlinear transport," *Physics Reports*, vol. 357, no. 1, pp. 1–11, 2002.
- [21] F. Feldmann, M. Bivour, C. Reichel, H. Steinkemper, M. Hermle, and S. W. Glunz, "Tunnel oxide passivated contacts as an alternative to partial rear contacts," *Solar Energy Materials and Solar Cells*, vol. 131, pp. 46–50, 2014.

- [22] F. Feldmann, M. Simon, M. Bivour, C. Reichel, M. Hermle, and S. W. Glunz, "Efficient carrier-selective p- and n-contacts for Si solar cells," *Solar Energy Materials and Solar Cells*, vol. 131, pp. 100–104, 2014.
- [23] T. Higa, R. Ishikawa, S. Miyajima, and M. Konagai, "Properties of Si/SiO₂ superlattice nanodisc array prepared by nanosphere lithography," in *Next Generation Technologies for Solar Energy Conversion V*, vol. 91780 of *Proceedings of SPIE*, San Diego, Calif, USA, August 2014.
- [24] H. S. Radhakrishnan, R. Martini, V. Depauw et al., "Kerfless layer-transfer of thin epitaxial silicon foils using novel multiple layer porous silicon stacks with near 100% detachment yield and large minority carrier diffusion lengths," *Solar Energy Materials and Solar Cells*, vol. 135, pp. 113–123, 2015.
- [25] P. Löper, D. Stüwe, M. Künle et al., "A membrane device for substrate-free photovoltaic characterization of quantum dot based p-i-n solar cells," *Advanced Materials*, vol. 24, no. 23, pp. 3124–3129, 2012.
- [26] S. Yamada, Y. Kurokawa, S. Miyajima, and M. Konagai, "Improvement of electrical properties of silicon quantum dot superlattice solar cells with diffusion barrier layers," *Japanese Journal of Applied Physics*, vol. 52, no. 4, Article ID 04CR02, 2013.
- [27] A. N. Corpus-Mendoza, M. M. De Souza, and F. U. Hamelmann, "Design of schottky contacts for optimum performance of thin-film silicon solar cells," *IEEE Journal of Photovoltaics*, vol. 5, no. 1, pp. 22–27, 2015.
- [28] R. V. K. Chavali, J. R. Wilcox, B. Ray, J. L. Gray, and M. A. Alam, "Correlated nonideal effects of dark and light I–V characteristics in a-Si/c-Si heterojunction solar cells," *IEEE Journal of Photovoltaics*, vol. 4, no. 3, pp. 763–771, 2014.



Hindawi

Submit your manuscripts at
<http://www.hindawi.com>

